Sensors and Actuators A 189 (2013) 409–419

Contents lists available at SciVerse ScienceDirect

Sensors and Actuators A: Physical

journal homepage: www.elsevier.com/locate/sna

Applying a hybrid DSMC/Navier–Stokes frame to explore the effect of splitter catalyst plates in micro/nanopropulsion systems

Masoud Darbandi[a,*], Ehsan Roohi[b]

[a] Department of Aerospace Engineering, Institute for Nanoscience and Nanotechnology, Center of Excellence in Aerospace Systems, Sharif University of Technology, P.O. Box 11365-8639, Tehran, Iran
[b] Department of Mechanical Engineering, Faculty of Engineering, Ferdowsi University of Mashhad, P.O. Box 91775-1111, Mashhad, Iran

ARTICLE INFO

Article history:
Received 8 December 2011
Received in revised form 6 September 2012
Accepted 7 September 2012
Available online xxx

Keywords:
MEMS
NEMS
DSMC
Cold-gas thrusters
Navier–Stokes
Hybrid algorithm
Micropropulsion systems
Nanopropulsion systems
Splitter plates
Catalyst plates
OpenFOAM

ABSTRACT

In this study, we apply a hybrid direct simulation Monte Carlo (DSMC)/Navier–Stokes (NS) frame to simulate the effects of catalyst or splitter plates in propulsive efficiency of micro/nanopropulsion systems. Our hybrid frame uses the local Knudsen number based on the gradient of the flow properties (Kn_{GLL}) to distinct the continuum and molecular regions. This frame also uses the state-based coupling (Dirichlet–Dirichlet boundary-condition coupling) to transfer the information between the two regions. We simulate typical micro/nanopropulsion systems consisting of channels, catalyst or splitter plates, and convergent–divergent nozzles. According to the Kn_{GLL}, we apply the NS solver to the channel including the splitter plates and the convergent part of the micro/nanopropulsion system and the DSMC solver to the divergent part of the system. In microscales, we find that the nozzle geometry can affect the system propulsive efficiency considerably. Additionally, the catalyst splitter plates can enhance the stagnation temperature upstream of the nozzle inlet and subsequently increase the overall specific impulse of the propulsion system. Furthermore, the inlet channel and the overall system sizes can affect the propulsive efficiency of the system, thrust force, and the specific impulse. However, a high viscous force in nanoscale propulsion systems does not permit the flow to meet the chocking condition at the nozzle throat. This limit decreases the propulsive force per unit area in the nanopropulsion systems considerably.

1. Introduction

As is predicted, the future small-sized spacecrafts need efficient propulsion systems to enable many of their proposed missions. On the other hand, the future micro/nanospacecrafts need significant propulsion capability in order to guarantee a high level of maneuverability. As is known, the micro/nanopropulsive systems can provide power for the mission or orbit control of micro/nanosatellites. These systems usually provide a low-level thrust in the order of 1 mN. Therefore, efficient simulation of micro/nanopropulsive systems is crucial for precise design of small-scale satellites. As the characteristic length of geometry decreases at micro/nanoscale, the rarefaction effects become serious. To describe the degree of gas flow rarefaction at the micro/nanoscale, Knudsen number is defined as the ratio of mean free path of gas molecules, λ, to a characteristic length in the flow field, L, i.e., $Kn = \lambda/L$. According to this definition, the rarefaction regimes can be categorized to slip ($0.001 < Kn < 0.1$), transition ($0.1 < Kn < 10$), and free molecular ($Kn > 10$) ones. There are different methods to simulate rarefied micro/nanoflow regimes. The Navier–Stokes (NS) solutions are valid for the slip regime if the velocity slip and temperature jump boundary conditions are suitably imposed. Alternatively, the direct simulation Monte Carlo (DSMC) [1] is a powerful numerical approach to solve the fluid dynamics problems in the entire rarefaction regimes. However, the computational cost of DSMC is controversial as the flow approaches the continuum regime. In continuum flow fields, the NS equations are a better choice to simulate the flow field efficiently. Considering the above points, efficient simulation of gas flow fields with considerable length scale variations needs employing advanced schemes such as a hybrid DSMC–NS frame. In a hybrid DSMC–NS frame, the molecular solver simulates the rarefied gas flow regions and the continuum solver is used to simulate flow of molecules in the near-equilibrium regions.

Our literature survey shows that the simulation of micro/nanopropulsion systems have been mostly performed using an individual either DSMC or NS solver. Additionally, such investigations are limited to simple nozzle geometries rather than a complete propulsive system. Bayt [2] used the finite volume Navier–Stokes simulations and studied the effects of viscous boundary layer on the propulsive performance of small-scale

* Corresponding author. Tel.: +98 21 6616 4644; fax: +98 21 6602 2731.
E-mail address: darbandi@sharif.edu (M. Darbandi).
URL: http://sharif.edu/ darbandi/ (M. Darbandi).

0924-4247/$ – see front matter © 2012 Elsevier B.V. All rights reserved.
http://dx.doi.org/10.1016/j.sna.2012.09.005

nozzles. He reported that the propulsive efficiency of a micronozzle decreases with the decrease of Reynolds number as the boundary layer thickness increases. Boyd et al. [3] studied the micronozzle employed in GP-B spacecraft using DSMC. Generally, the GP-B spacecraft uses cold gas micropropulsion to perform its mission [4]. Boyd et al. [3] also studied the effects of back-pressure on the flow field inside the micronozzle. Their results were in good agreement with the experiments. Zelesnik et al. [5] studied the effects of nozzle geometry and stagnation temperature on the propulsive force of nozzles at low Reynolds number regimes. They showed that conical nozzles provide the maximum thrust as they permit maximum amount of mass flux compared with the bell-shaped nozzles for the same inlet conditions. Ivanov and Markelov [6] simulated axisymmetric micronozzles using DSMC. They used a hybrid frame, which used the NS solver in near equilibrium regions and the DSMC solver in the rarefied regions. Hitt et al. [7] focused on MEMS-based satellite micropropulsion systems using catalyzed hydrogen peroxide decomposition. They presented different micropropulsion systems constructed in NASA Goddard Space Flight Centre. They performed different experimental tests to measure the decomposition efficiencies of hydrogen peroxide propellant. Alexeenko et al. [8] simulated flow through axisymmetric and 3D micronozzles using the DSMC and NS solvers. They observed that the viscous effects dominate the gas expansion and reduce the thrust due to significant wall viscous effects. Xie [9] simulated low Knudsen number micronozzle flows using DSMC and solving the NS equations. He measured the dependency of mass flow rate on the pressure differences. Titov et al. [10] simulated the flow through 3D micronozzles considering Reynolds numbers from 200 to 2000. They used a collision limiter DSMC approach (eDSMC) to extend the applicability of direct simulation Monte Carlo to the continuum regime in treating micronozzles flows. The results of eDSMC method were compared with those of the NS computations for a three-dimensional nozzle with high stagnation pressure and temperature magnitudes. There were good agreements between the solutions of eDSMC and Euler governing equations. La Torre et al. [11] studied the effects of wavy surface roughness on the performance of micronozzles. They simulated conical convergent–divergent micronozzles and reported formation and reflection of several weak shocks due to the surface roughness. Moríñigo and Hermida-Quesada [12] performed steady-state performance analysis of a flat-shaped micronozzle in under-expanded cold and hot-gas operations using the NS equations subject to velocity slip and temperature jump boundary conditions. They concluded that the friction force and heat transfer over the side-walls characterize the MEMS-class nozzles. Darbandi and Roohi [13] used an unstructured DSMC solver to simulate a wide range of rarefaction regimes from subsonic to supersonic flows through micro/nanoscale converging–diverging nozzles. They studied the effects of back-pressure, gas/surface interactions (diffuse/specular reflections), and Knudsen number on the flow field in micro/nanoscale nozzles.

Our literature survey shows that the numerical simulation of micro/nanopropulsive systems has been mostly restricted to the nozzle geometries. Meanwhile, the real micro/nanopropulsive systems consist of different components, which may affect the overall propulsive performance of the system. Therefore, the main objective of the current study has been to provide a deeper understanding of the flow behavior in a tentative micro/nanoscale propulsive system designed and constructed in NASA Goddard Space Flight Centre, see Ref. [7]. We use a hybrid DSMC–NS algorithm incorporated with a state-based coupling to perform our simulation efficiently. Using our experience in developing different continuum [14–20] and molecular [13,21–25] solvers, we extend a hybrid DSMC–NS method in the context of OpenFOAM [26]. We use "dsmcFoam" solver as our molecular solver [25]. This solver was developed as a joint venture research work performed by the current authors from Sharif University of Technology, the faculty members of University of Strathclyde and the code developers in the OpenCFD Ltd.

The rest of this paper is organized as follows. Section 2 describes the DSMC and NS solvers as well as our state-based hybrid frame. Section 3 presents the results of solving rarefied gas flows in different micro/nanopropulsive systems using our hybrid solver. The concluding remarks are provided in Section 4.

2. Computational approach

2.1. The DSMC solver

DSMC is a numerical tool to solve the Boltzmann equation based on direct statistical simulation of the molecular processes described by the kinetic theory [1]. It is considered as a particle method in which each particle represents a large bulk of real gas molecules. The primary principle of DSMC is to decouple the motion and collision of particles during one time step. The implementation of DSMC needs breaking down the computational domain into a collection of grid cells. The cells are divided into subcells in each direction. The subcells are then utilized to facilitate the selection of collision pairs. Accurate DSMC solution requires some constraints on the cell size, time step, and number of particles. A random selection of particles from a cell for binary collisions requires that the cell size to be a small fraction of the gas mean free path. The decoupling between the particles movement and collisions is correct if the time step is a small fraction of the mean collision time. Indeed, the number of particles per cell should be high enough, around 20, to avoid repeated binary collisions between the same particles. To solve a stationary problem with DSMC, an arbitrary initial state of gas particles is first specified and the desired boundary conditions are imposed in the entire computational domain at time zero. Second, the particles movement and the binary collisions are performed separately. After achieving the steady flow condition, sampling of molecular properties is fulfilled within each cell during a sufficiently long time to avoid statistical scattering. All thermodynamic parameters such as temperature, velocity, density, and pressure are then determined from this time-averaged data.

As stated, we use a general DSMC solver named dsmcFoam [25] under the framework of OpenFOAM. OpenFOAM is a flexible set of efficient, object-oriented C++ modules for solving complex fluid flows [26]. It is mainly a finite-volume package designed to solve systems of differential equations in arbitrary geometries. In developing dsmcFoam, we benefited from the features of OpenFOAM such as particle tracking in unstructured, arbitrary, and polyhedral meshes. dsmcFoam can model arbitrary geometries and arbitrary number of gas species. dsmcFoam uses the Variable Hard Sphere (VHS) collision model and Larsen–Borgnakke internal energy redistribution model [1] to perform inter-molecular collisions. The boundary walls are treated as diffuse reflectors using the full momentum and thermal accommodation coefficients.

2.2. The NS equations and solver

The NS equations can be derived from the Chapman–Enskog expansion of the Boltzmann equation. These equations, namely conservation of mass, moment and total energy, are expressed as [26]

$$\frac{\partial \rho}{\partial t} + \nabla \cdot [\mathbf{V}\rho] = 0 \tag{1}$$

$$\frac{\partial (\rho \mathbf{V})}{\partial t} + \nabla \cdot [\mathbf{V}(\rho \mathbf{V})] + \nabla p + \nabla \cdot \boldsymbol{\tau} = 0 \tag{2}$$

$$\frac{\partial(\rho E)}{\partial t} + \nabla \cdot [\mathbf{V}(\rho E)] + \nabla \cdot [\mathbf{V}p] + \nabla \cdot (\boldsymbol{\tau} \cdot \mathbf{V}) + \nabla \cdot \mathbf{q} = 0 \quad (3)$$

where ρ is the mass density, p is the pressure, $E = e + |\mathbf{V}^2|/2$ is the total energy, e is the internal energy per unit mass, $\mathbf{q}$ is the diffusive flux of heat and $\boldsymbol{\tau}$ is the shear stress tensor. Using the Stokes law, the stress tensor can be described by

$$\boldsymbol{\tau} = \mu \, \mathrm{dev}(\nabla \mathbf{V} + (\nabla \mathbf{V})^T) \quad (4)$$

where dev means the deviatoric of the tensor, μ is the dynamic viscosity, and the superscript T denotes the transpose. The Fourier's law represents the diffusive heat flux as follows:

$$\mathbf{q} = -k \ \nabla T \quad (5)$$

where k is the thermal conductivity. In order to consider rarefaction effects, the first-order velocity slip and temperature jump boundary conditions are applied at the walls as follows [13]:

$$\mathbf{V}_g - \mathbf{V}_w = -\frac{2-\sigma_u}{\sigma_u}\lambda \nabla_n (\mathbf{S} \cdot \mathbf{V}) - \frac{2-\sigma_u}{\sigma_u}\frac{\lambda}{\mu}\mathbf{S} \cdot (\mathbf{n} \cdot \boldsymbol{\Pi}_{mc}) - \frac{3}{4}\frac{\mu}{\rho}\frac{\mathbf{S} \cdot \nabla T}{T} \quad (6)$$

$$T_g - T_w = -\frac{2-\sigma_T}{\sigma_T}\frac{2\gamma}{(\gamma+1)\mathrm{Pr}}\lambda \nabla_n T \quad (7)$$

where $\mathbf{n}$ represents the unit normal vector to the surface. Additionally, the subscripts g and w refer to gas adjacent to wall and wall, respectively. σ_u and σ_T are the tangential momentum and thermal accommodation coefficient, respectively. γ is the specific heat ratio and Pr is the Prandtl number. The tensor $\mathbf{S} = \mathbf{I} - \mathbf{nn}$, considering $\mathbf{I}$ as the identity tensor, removes the normal components of any non-scalar field. Additionally, $\boldsymbol{\Pi}_{mc}$ is expressed as

$$\boldsymbol{\Pi}_{mc} = \mu(\nabla \mathbf{V})^T - \left(\frac{2}{3}\right)\mathbf{I}_{tr}(\nabla \mathbf{V}) \quad (8)$$

where the subscript tr denotes the trace. Both accommodation coefficients have been considered as unity to simulate diffuse reflector walls. The second and third terms at the RHS of Eq. (6) consider the effects of boundary curvature and thermal creeps on the velocity slip, respectively. We use the power law relation to present gas viscosity as a function of temperature magnitude as follows:

$$\mu = \mu_{\mathrm{ref}}\left(\frac{T}{T_{\mathrm{ref}}}\right)^{\omega} \quad (9)$$

$$\mu_{\mathrm{ref}} = \frac{15\sqrt{m\pi k T_{\mathrm{ref}}}}{2\pi d_{\mathrm{ref}}^2 (5-2\omega)(7-2\omega)} \quad (10)$$

where ω is the macroscopic viscosity temperature exponent, d is the molecular diameter, and $k = 1.38 \times 10^{-23}$ is the Boltzmann constant. For nitrogen gas, they are $\omega = 0.74$ and $d = 4.17 \times 10^{-10}$. We apply the power law relation to be consistent with the VHS model used in our DSMC solver.

In this work, we use "rhoCentralFoam" module of OpenFOAM as a NS solver [26]. rhoCentralFoam is an explicit density-based solver for simulating viscous compressible flows. It benefits from a Godunov-like central-upwind scheme. The space discretization has a second-order accuracy based on reconstruction of the primitive pressure, velocity, and temperature variables. Our time integration employs the first-order forward scheme.

2.3. The hybrid strategy

There are two main issues, which need to be addressed by any hybrid algorithm. They are the locations of continuum–molecular interface and the equilibrium breakdown parameter. Any hybrid solver should enhance its computational efficiency by restricting the DSMC solutions suitably to non-equilibrium regions. Usually, a continuum breakdown parameter is applied to locate the interface. This parameter can be derived from the relation between the Boltzmann and NS equations. Different breakdown parameters have been suggested. One is the local Knudsen number based on the gradients local length (GLL) of the flow properties. It is defined as

$$\mathrm{Kn}_{\mathrm{GLL}\phi} = \frac{\lambda}{\phi}|\nabla \phi| \quad (11)$$

where ϕ is an arbitrary flow parameter and $\mathrm{Kn}_{\mathrm{GLL}} = \max(\mathrm{Kn}_{\mathrm{GLL},\rho}, \mathrm{Kn}_{\mathrm{GLL,V}}, \mathrm{Kn}_{\mathrm{GLL,T}})$ [27]. $\mathrm{Kn}_{\mathrm{GLL,V}}$ is computed based on the velocity magnitude. The local mean free path used in the gradient-length Knudsen number is calculated using the VHS formula as follows [1]:

$$\lambda = \frac{2(5-2\omega)(7-2\omega)}{15}\sqrt{\frac{m}{2\pi k T}\left(\frac{\mu}{\rho}\right)} \quad (12)$$

Another breakdown parameter is the parameter B, which is taken as the maximum value for the shear stress and heat flux magnitudes. It is given by

$$B = \max(|q_i^*||\tau_{ij}^*|) \quad (13)$$

where

$$q_i^* = \left(\frac{\kappa}{P}\right)\left(\frac{2m}{kT}\right)^{0.5}\nabla T \quad (14)$$

and

$$\tau_{ij}^* = \left(\frac{\mu}{P}\right)(\mathbf{V}_{i,j} + \mathbf{V}_{j,i} - \mathbf{V}_{k,k}\delta_{ij}) \quad (15)$$

where indices i, j, and k stand for the three velocity components. The equilibrium breakdown occurs whenever $\mathrm{Kn}_{\mathrm{GLL}} > 0.05$ [27] or if $B = 0.1$ [28]. In this work, we used $\mathrm{Kn}_{\mathrm{GLL}}$ as the breakdown parameter to determine the continuum–molecular interface. A small overlap region is considered at the interface between the two solvers. This region is solved with both solvers. The benefit of using the overlap region is that the hybrid solution is not influenced by the exact position of interface.

Our hybrid cycle is based on the scheme suggested by Schwartzentruber et al. [29], as follows:

1. Obtain the NS solution for the entire domain (this solution is inaccurate in non-equilibrium regions but it is acceptable in the near-equilibrium regions),
2. Apply the breakdown parameter to the above solution and specify the non-equilibrium (DSMC) and equilibrium (NS) regions,
3. Use the DSMC solver to obtain solution in the rarefied and overlap regions, and similarly, solve the NS solver in the near-equilibrium region,
4. Reapply the breakdown parameter to both regions and change the interface between these two regions if it is necessary, and
5. Repeat steps 3 and 4 unless the breakdown parameter indicates that the interface location does not change.

3. Results and discussion

In this section, we apply our hybrid NS–DSMC solver to a number of micro/nanopropulsion systems. However, it is instructive to investigate the flow field inside a simple micronozzle using our hybrid frame before simulating any complete propulsive system. Indeed, the micronozzle simulation would provide a suitable experience to set up our hybrid frame in a more complicated propulsive geometry more effectively. Next, we apply the hybrid solver to simulate three micropropulsion test cases with and without splitter plates. Eventually, we analyze two nanopropulsion systems with

Table 1
Detailed information of simulated micro/nanopropulsion systems.

Type	Case	System description	H_{inlet}	$L_{channel}/H_{inlet}$	L_{nozzle}/H_{inlet}	H_{throat}/H_{inlet}	U_{inlet} (m/s)	Kn_{inlet}
Micro	1	Without splitter plates	50 μm	6	2	0.1	150	0.003
	2	With splitter plates, T_p = 300 K						0.014
	3	With splitter plates, T_p = 600 K						0.013
Nano	4	With splitter plates, T_p = 300 K	7.5 nm	325	150	25	100	0.15
	5	With splitter plates, T_p = 300 K	75 nm	65	10	5	100	0.15

the catalyst plates. The details of these five test cases are provided in Table 1. For all simulated micro/nanopropulsive systems, the working gas is nitrogen.

3.1. Test 1 – microscale nozzle

Fig. 1 shows the geometry of our chosen micronozzle. Considering a symmetric geometry and flow, we only solve one-half of the solution domain. The throat height H_t is 15 μm. The inlet Knudsen number is $Kn_{in} = 7.5 \times 10^{-4}$. The inlet boundary conditions are specified as a static pressure of P_{in} = 1 atm, a total pressure of $P_{t,in}$ = 1.19 atm, and an inlet temperature of T_{in} = 300 K. The wall temperature is specified as T_{wall} = 300 K. Since the flow is supersonic at the nozzle outlet, we do not specify any parameter there.

3.1.1. Validation of the DSMC solver

Since there is no experimental result for the micro/ nanopropulsion system, we compare our numerical solution with the DSMC solution of Liu et al. [30]. This helps to verify the accuracy of our hybrid solver. We use a structured grid of 400 × 150 to discretize the entire nozzle domain. This grid was chosen after a careful grid refinement study. Fig. 2 presents the centerline temperature and Mach number distributions and compares them with those presented in Ref. [30]. The lengths are nondimensionalized with respect to the nozzle length $L_n = L_1 + L_2$ in this figure. As is seen, there are suitable agreements between the current solutions and those of reference. As is observed, we have performed our DSMC simulation using two different number of particles per cells (NPC), i.e., NPC = 15 and NPC = 30. The achieved solutions indicate that there is negligible dependency on the NPC magnitude. The results of Fig. 2 are trustworthy and we can use our DSMC solver to simulate our proposed micro/nanopropulsion systems.

3.1.2. Validation of the hybrid solver

At this stage, we would like to verify our hybrid DSMC–NS simulator. As the first step of our hybrid frame, it is necessary to determine the continuum and rarefied regions using a suitable parameter like the local Knudsen number magnitude. Fig. 3 shows the local Knudsen number based on the density predicted by the continuum and molecular solvers. In fact, $Kn_{GLL,\rho}$ is the maximum local Knudsen number. As is observed, the boundary layer regions at the throat and the divergent section of micronozzle are the places where the local Knudsen number exceeds the threshold value of 0.05.

As the ongoing flow expands, it becomes more rarefied and consequently, the non-equilibrium region increases effectively. From our previous experiences, the NS solution of the flow field at the divergent section of the nozzle is not accurate even at the nozzle centerline [13]. The above study indicates that it is better to solve the entire divergent section using our DSMC solver and use the NS solver to solve the convergent section. The additional benefit of this division is that the low speed region of the nozzle (located in the convergent section) is not solved using the DSMC solver. As is known, DSMC solution needs more computational time and sample size in solving low speed flows [21]. Fig. 4 shows the grid used for the discretization of the continuum and molecular regions. We use a grid with (80 × 150) structured meshes in the convergent section and a grid with (120 × 80) cells in the divergent section.

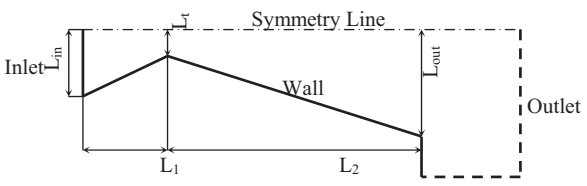

Fig. 1. Micronozzle geometry including the imposed buffer zone and the general implemented boundary conditions.

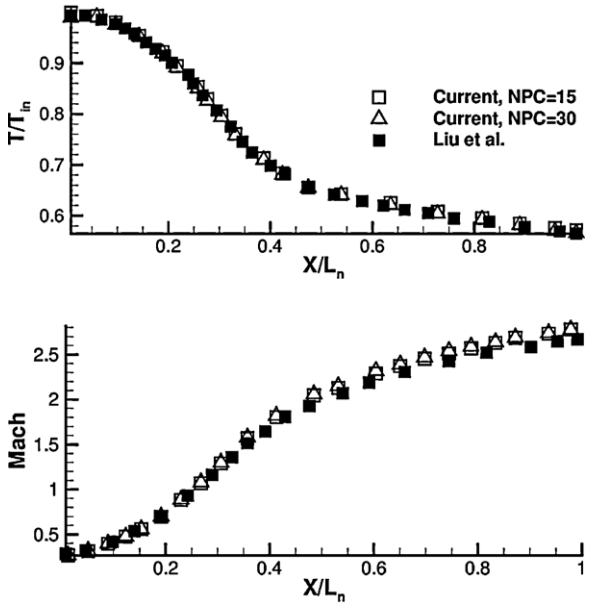

Fig. 2. Presenting the current temperature and Mach number distributions at the micronozzle centerline and comparing them with the results of Liu et al. [30].

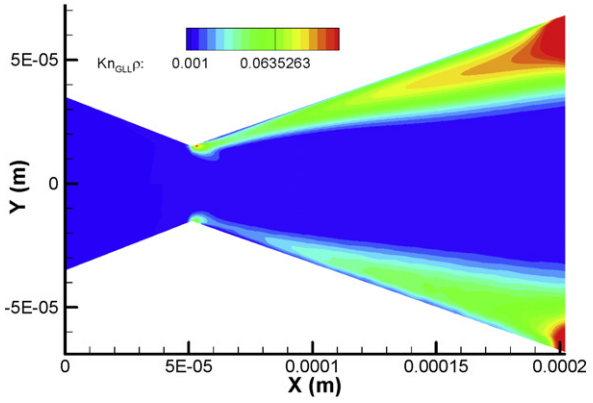

Fig. 3. Comparison of local Knudsen number based on the density predicted by the continuum (top region) and molecular (bottom) solvers.

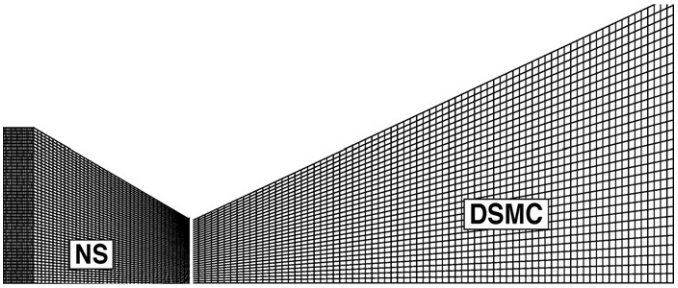

Fig. 4. The utilized grid in the NS and the DSMC regions.

These grids are selected after a careful grid convergence study, see Ref. [13]. We set total pressure, temperature, and pressure at the inlet of the convergent section. The back-pressure at the end of convergent section is provided by the DSMC solution and is implemented by the NS solver. Alternatively, we use the NS solution to provide the inlet boundary conditions at the start of the divergent section, i.e., we set the supersonic velocity, temperature, and number density. These data are used to sample the velocity of incoming molecules and can help to calculate the fluxes to the divergent section. We do not set any boundary conditions at the outlet of nozzle, as the flow is supersonic there.

Fig. 5 shows the velocity profile at the nozzle throat using the NS and DSMC solvers individually. It is observed that both solutions are the same at the throat except a small discrepancy observed nearby the nozzle wall. In fact, our experience has shown that if the discrepancy between the DSMC and NS solutions is limited to a small region at their interface, the hybrid solver will eventually converge to an accurate solution. It is because the number of particles entering into the domain, i.e., through the boundary cells located at those small regions, is much less than that of the particles entering into the domain through the rest of boundary cells located at the interface. On the other hand, these numbers are much less than the number of particles already exist in the entire hybrid interior domain. Therefore, the slight inaccuracy caused by these particles would disappeared during the hybrid simulation. In other words, the hybrid frame solution would converge to an accurate solution eventually despite a slight inaccuracy introduced at the hybrid interface.

Fig. 6 shows the variation of temperature at the micronozzle centerline derived by the hybrid, NS, and DSMC solvers. It is observed that the hybrid solution agrees well with the pure DSMC solution in the divergent section of nozzle although the boundary conditions at the inlet of the divergent section are taken from the NS solutions. Of importance, the discrepancy observed nearby the wall, see Fig. 5, has not affected the hybrid solution at all.

The main benefit of hybrid solver is the reduction in the computational time. The computational time for full DSMC simulation of the investigated micronozzle is around 38 h using an Intel Core Due T6400 Hz laptop with 3 GB RAM. This time is reduced to 26 h for

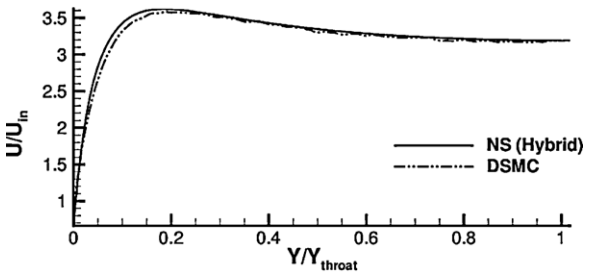

Fig. 5. Normalized velocity profile at the nozzle throat using the NS and DSMC solvers.

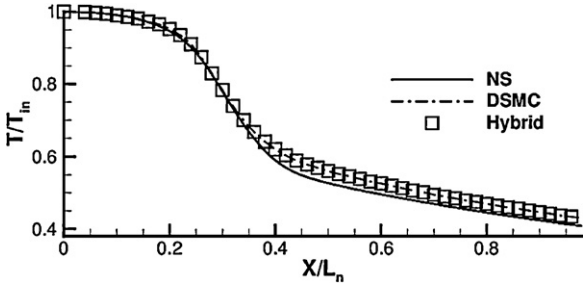

Fig. 6. Temperature distribution at the nozzle centerline derived from the continuum, molecular, and hybrid solutions.

the hybrid solver (24 h for the DSMC solver, 2 h for the NS solver). Therefore, the required computational time for our hybrid solver was about 68% of our individual DSMC simulator.

3.2. Test 2 – micropropulsion system

The next step in evaluating our developed hybrid algorithm is to simulate a micropropulsion system. The chosen micropropulsion system is shown in Fig. 7. This geometry is inspired in the microdevice system originally manufactured and tested by Hitt et al. [7]; but not exactly with the same size and components. We perform our simulations for two different micropropulsion system configurations. The first system consists of a microchannel, a micronozzle, and an exit buffer zone, see Fig. 7(a). The second system consists of the first system in addition to a bundle of catalyst splitter plates inside the microchannel; see Fig. 7(b). We put 10 splitter plates, whose sizes are $(2.5 \times 150)\,\mu$m, inside the channel. The gap size between each two plates is 2.5 μm. In all of our micro/nanopropulsion system test cases, we imposed a temperature of 300 K and an inlet velocity, whose details are provided in Table 1. One may become confused with using a velocity definition instead of a pressure specification at the channel inlet. In other words, one may say, "controlling the feeding pressure has more sense in micro/nano thrusters." The reason for choosing the velocity (instead of the pressure) as the inlet boundary condition is optional and not mandatory. It is because unlike our experience in solving a nozzle configuration, we observed that the micro/nanopropulsion system would converge more smoothly if we specify the velocity (instead of pressure) at the inlet. However, one should note that we derived this velocity magnitude from the total and static

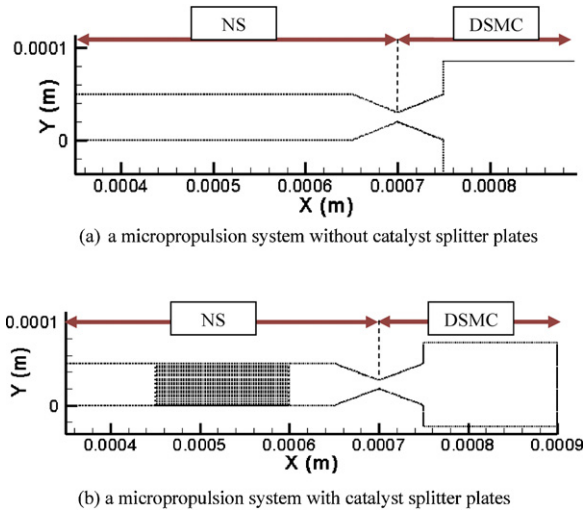

Fig. 7. Two chosen micropropulsion systems without (a) and with (b) the catalyst splitter plates.

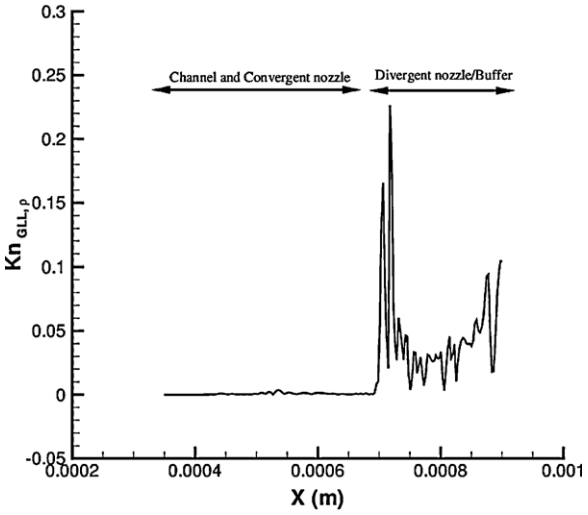

Fig. 8. Variation of the $Kn_{GLL,\rho}$ at the micropropulsion system centerline, Case 1.

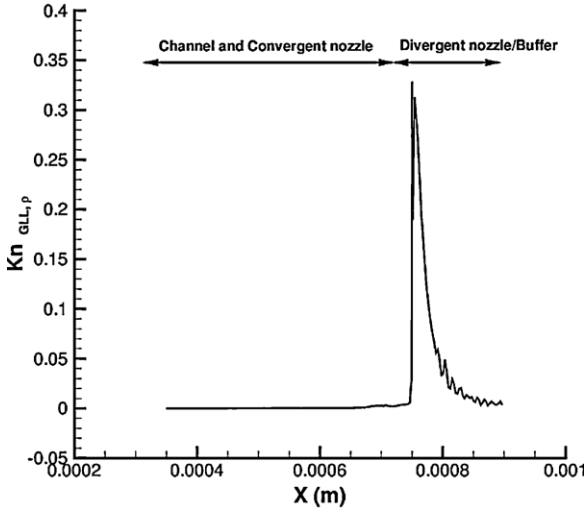

Fig. 10. Variation of the $Kn_{GLL,\rho}$ at the micropropulsion system, Case 2.

pressure values, which were specified in advance at the inlet of channel. Therefore, there is absolutely no difference choosing either velocity or pressure at the inlet in our test case. In other words, there is no conflict with the fact that the feeding pressure controls the thrust of the system in our test cases.

3.2.1. Case 1

The inlet velocity for Case 1 is 150 m/s and the inlet/wall temperature is 300 K. The inlet Knudsen number, based on the channel height, is 0.003. Our local Knudsen number study resulted in the same domain decomposition as suggested in Section 3.1. As shown in Fig. 8, the channel and convergent section of the nozzle can be treated as the equilibrium regions because the Kn_{GLL} has a negligible value and almost constant. Therefore, these regions should be solved using the NS solver. Alternatively, the divergent section of the nozzle and the buffer zone are in the rarefied region and should be simulated using the DSMC solver.

Fig. 9 shows the Mach number and temperature contours inside the micropropulsion system. The regions specified to the NS and DSMC solvers are indicated in this figure as well. It is observed that the Mach number expansion mostly occurs in the divergent section and the buffer zone. Meanwhile, the temperature variations start from the middle section of the channel. The gas flow is heated more as approaches the convergent section of the nozzle and reaches to the highest temperature at the nozzle throat. As the flow expands in the divergent section, the gas cools and reaches to a low value around 50 K.

3.2.2. Case 2

The inlet Knudsen number is 0.014 in this case. We do not consider the effects of chemical reactions but focus on the effects of splitter plates on the fluid dynamics and heat transfer of the micropropulsion system. The key effect of using catalyst splitter plates is the increase of the total friction force of the system. As is shown in Fig. 10, the local Knudsen number variation is similar to Case 1. Although insertion of the splitter plates decreases the size of flow passage, there is no sensible change in the local Knudsen number along the splitter because there is little variations in flow properties along these plates. Therefore, splitting the DSMC and NS regions is the same as Case 1.

Fig. 11 shows the Mach and temperature contours calculated by the hybrid solver. The maximum value of Mach number is lower than that calculated in Case 1. The temperature variations of this case also show a lower value at the throat of the micronozzle if it is compared with Case 1.

Fig. 12 shows the profiles of different flow properties including the temperature, Mach number, static pressure, and velocity at various locations inside the micropropulsion system. The non-dimensional location $X/L = 0.45$ is at the microchannel, $X/L = 0.70$ is at the convergent section of the nozzle, $X/L = 0.82$ is at the divergent section, and $X/L = 0.85$ and $X/L = 90$ are placed in the buffer zone.

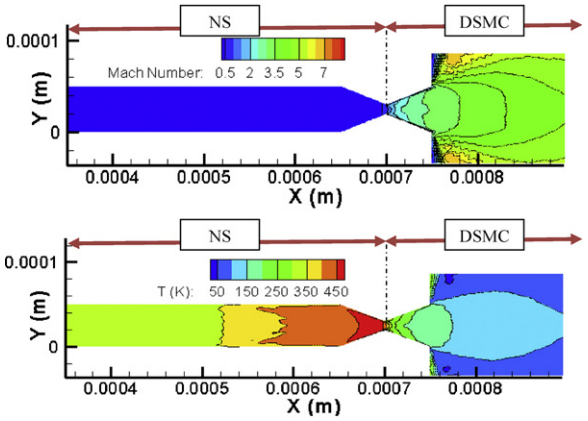

Fig. 9. Mach and temperature contours calculated by the hybrid solver, Case 1.

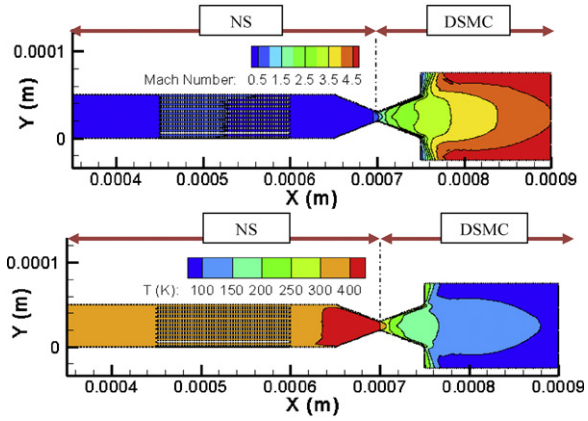

Fig. 11. Mach and temperature contours calculated by the hybrid solver, Case 2.

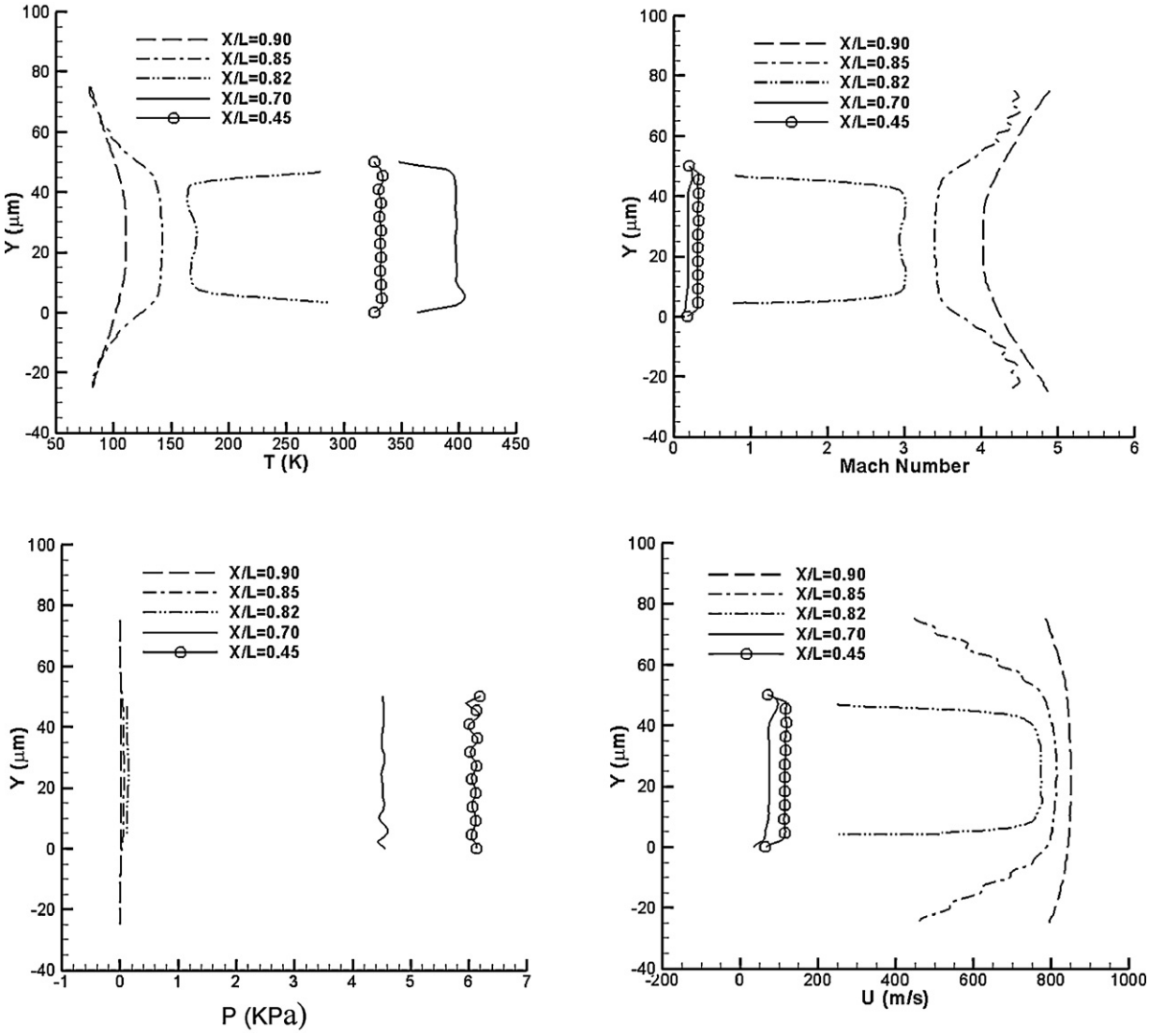

Fig. 12. Profiles of different flow properties at different chosen longitudinal locations in the micropropulsion system, Case 2.

Here, L denotes the entire axial length of the computational domain. It is observed that the temperature is constant at $X/L = 0.45$. It is about 340 K. It slightly decreases near the wall at this location. At $X/L = 0.70$, the temperature is again constant in the core region of the nozzle but there is a larger gradient near the wall comparing with that at $X/L = 0.45$. At the divergent part, $X/L = 0.82$, the core flow is colder than the gas adjacent to the wall. There is a bimodal behavior in temperature profile at this location, i.e., there is a slight increase in the temperature at the centerline of the nozzle. The same phenomenon has been reported for the rarefied Poiseuille flow [31]. As the flow expands in the buffer region, it becomes cooler. Mach number behavior is similar to the temperature one, i.e., we observe a bimodal behavior. It should be noted that the velocity profile does not show such a bimodal behavior at all. The velocity shows steeper gradient at the divergent section compared with that of the temperature profile. As the flow expands in the divergent section, it becomes uniform. However, the pressure profile is nearly constant along the micropropulsion system.

3.2.3. Comparison of Cases 1 and 2

Fig. 13 presents the flow field properties along the micropropulsion centerline for Cases 1 and 2 and compares them with each other. This figure illustrates the effect of using splitter plates on the gas flow properties. It is clearly observed that there is a considerable pressure reduction in the system as the splitter plates are inserted in the micropropulsion system.

At the beginning of the plates, there is a slight decrease in static pressure and temperature and a moderate increase in the velocity and Mach number magnitudes. Meanwhile, the temperature, Mach number and velocity are the same at the nozzle and buffer zones for both cases. Therefore, the splitter plates do not affect the gas flow-choking incident and the nozzle geometry determines the flow field behavior. Indeed, the splitter plates determine the upstream conditions, i.e., they change the inlet static pressure and flow field inside the channel. However, they do not affect the flow at the nozzle. In other words, the key configuration in this micropropulsion system is the geometry of micronozzle.

3.2.4. Case 3

The outcome of catalyst reactions in a real micropropulsion system is to heat the fluid. To modify our pervious test cases, we consider a splitter plate temperature of 600 K, which is much higher than the inlet flow and wall temperature, i.e., 300 K. Fig. 14 compares the distribution of flow properties at the centerline of two

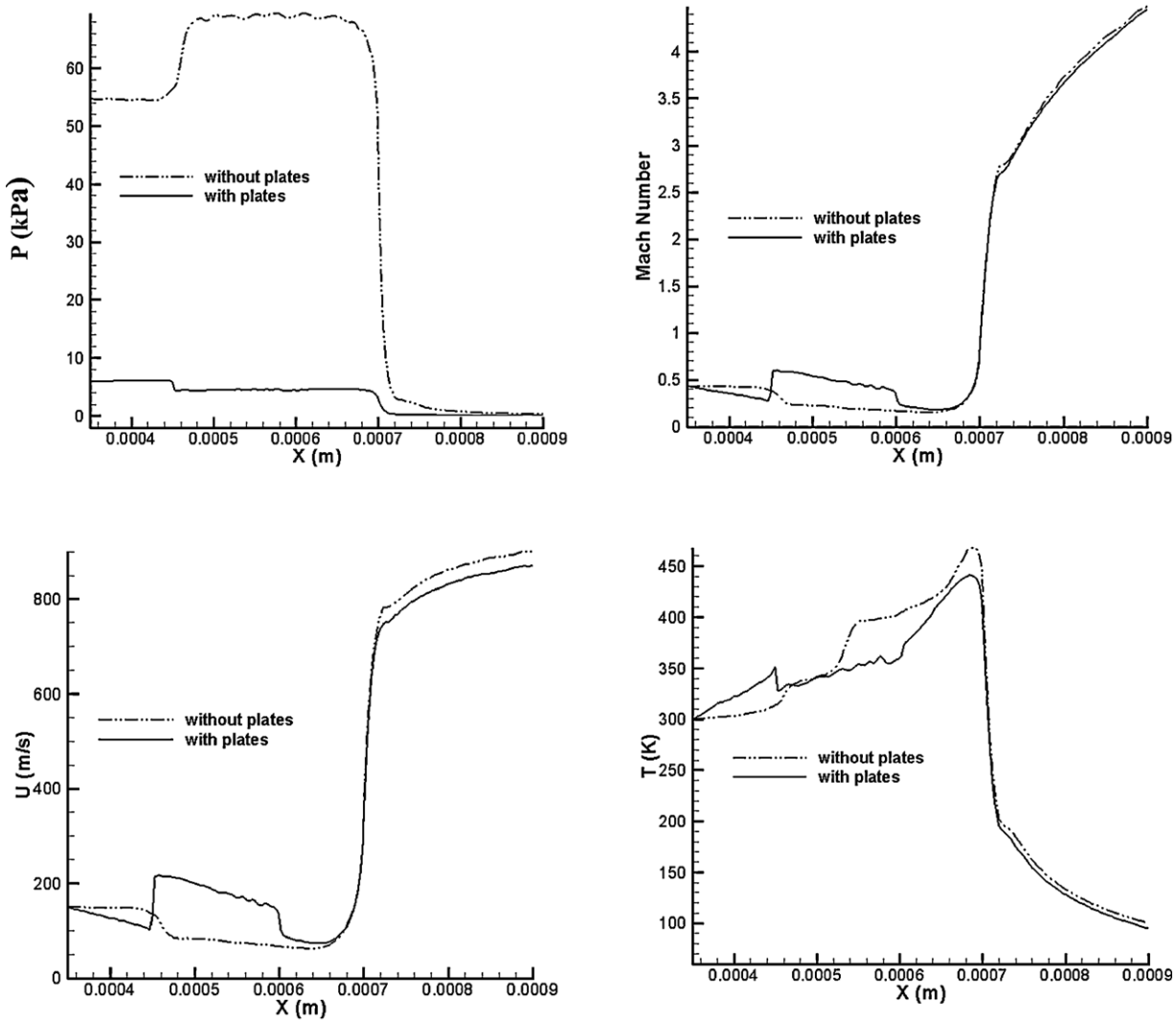

Fig. 13. Comparison of different flow properties along the centerline of micropropulsion systems, Cases 1 and 2.

micropropulsion systems, i.e., Cases 2 (T_p = 300 K) and 3 (T_p = 600 K). Complex interaction of heat transfer phenomenon with the friction forces determines the eventual behavior of the flow field in both cases. As is observed, the temperature increases linearly in the microchannel in Case 3. It reaches to a maximum value higher than the plate temperature, i.e., it reaches to 850 K. Similarly, the velocity increases linearly (but with a lighter step comparing with temperature) once the flow passes over the splitter plates. Meanwhile, the static pressure decreases linearly from around 4.4 kPa to 1.6 kPa over the splitter plates. In fact, the channel pressure loss is converted to the velocity and temperature increases. The velocity and temperature magnitudes at the micronozzle are higher for Case 3 than Case 2. Meanwhile, Mach number distribution (the ratio of velocity to temperature) is identical for both Cases 2 and 3 at the nozzle. It is observed that there is a velocity jump at the start of splitter plates and the flow decelerates over the plates in Case 2 due to the viscous forces. Meanwhile, the flow accelerates over the splitter plates in Case 3 due to a gas heating process.

Table 2
Performances of different micropropulsion systems, Cases 1–3.

System type	V_{exit} (m/s)	$\dot{m}$ (g/s)	F_t (mN)	I_{sp} (s)
Case 1	741	12	9.8	75.6
Case 2	721	8.3	5.9	73.6
Case 3	915	8.1	6.4	93.7

3.2.5. Performance comparison for Cases 2 and 3

Table 2 provides a quick comparison among the performances of three preceding micropropulsion systems. In this table, the thrust force is calculated from $F_t = \dot{m}V_{exit}$ and the thrust specific impulse is given by

$$I_{sp} = \frac{F_t}{\dot{m}g_0} \tag{16}$$

It is observed that the exit velocity and specific impulse are the highest for Case 3. Therefore, a higher catalyst plate's temperature would result in a higher specific impulse. Meanwhile, the maximum thrust force occurs for Case 1, where there are no splitter plates. Therefore, the inlet static pressure and mass flow rate would be the highest magnitudes in this case.

3.3. Test 3 – nanopropulsion systems

The next stage of our simulation considers the flow field study inside a nanopropulsion system. The details of chosen geometries are provided as Cases 4 and 5 in Table 1. The inlet and splitter temperature are fixed at 300 K. The inlet Knudsen number and velocity for both cases are set as 0.15 and 100 m/s, respectively. Since this

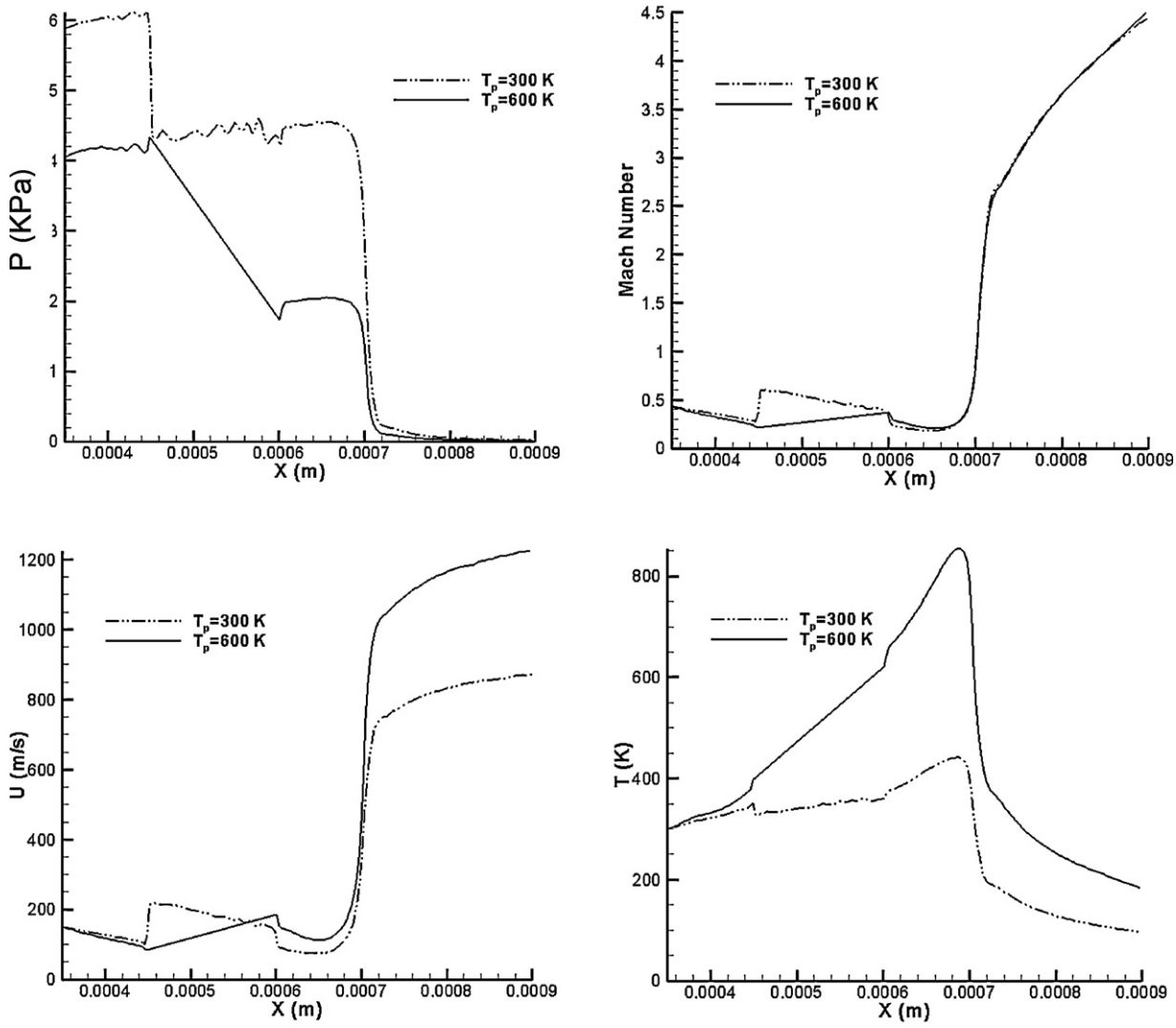

Fig. 14. Comparison of different flow properties along the centerline of micropropulsion systems, Cases 2 and 3.

test case is beyond the slip flow regime limit, we cannot apply hybrid frame for nanopropulsion system and should use individual DSMC solver for the whole flow region.

3.3.1. Case 4

Fig. 15 shows the Mach and temperature contours inside the nanopropulsion system. It is observed that the flow starts decelerating as it approaches the splitter plates. The Mach number is almost constant as the flow passes through the plates. The Mach number again increases as the flow reaches the nanonozzle throat, but the flow is not chocked. The decrease in Mach number is due to a high viscous force, which converts the inertial forces to the thermal field, as is shown in temperature contours. It is observed that the temperature increases as the flow reaches the splitter plate. The temperature is almost constant on the rest of the channel and nozzle but it expands at the buffer zone.

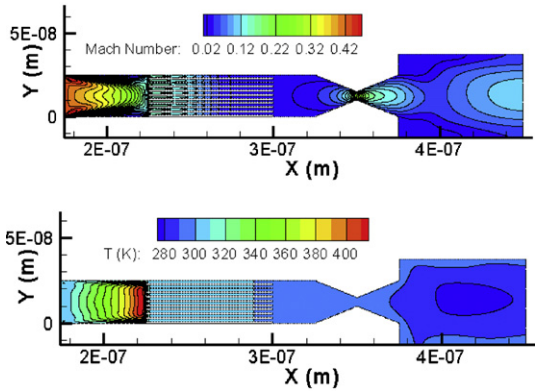

Fig. 15. Mach and temperature contours, Case 4.

3.3.2. Case 5

In Case 5, we consider another nanopropulsion system with larger inlet and throat sizes. The inlet and wall conditions are the same as the previous test case. The temperature and Mach number contours are shown in Fig. 16 for this case. Since the resisting viscous force is lower for this geometry, the Mach number decreases with a slower rate while the temperature increase is not as high as that in Case 4. Other flow characteristics are the same, e.g., the flow does not choke. Table 3 presents the performances of two presented nanopropulsion systems. As is observed, the nanopropulsion systems can provide small thrust force magnitudes in the order of milli-Newtons. Additionally, the system specific impulse and system exit velocity magnitudes are quite low compared with those of micro-propulsive systems, i.e., the exit velocity and the specific

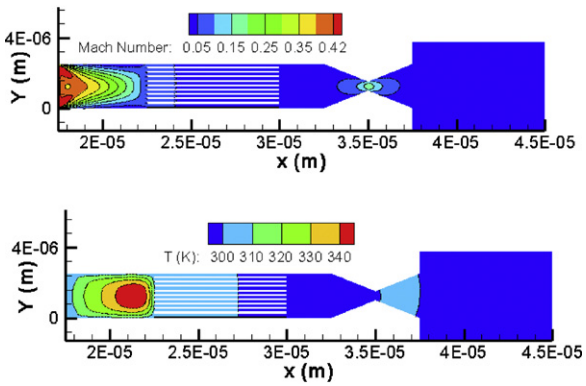

Fig. 16. Mach and temperature contours, Case 5.

Table 3
The performances of two considered nanopropulsion systems, Cases 4–5.

System type	V_{exit} (m/s)	$\dot{m}$ (g/s)	F_t (mN)	I_{sp} (s)
Case 4	12	0.60	7.2	1.22
Case 5	7	0.45	3.2	0.71

impulse are in the order of 10^1 and 10^0 mN, respectively. Therefore, it is evident that the nanopropulsion systems are suitable to be used in low-weight nanosatellite systems, which require low thrust and impulse levels.

4. Conclusion

We used a hybrid DSMC–NS frame to study the rarefied gas flow through different micro/nanopropulsive systems. We used the continuum solver of OpenFOAM, namely rhoCentralFoam, and developed a molecular solver, i.e., dsmcFoam to perform this study. The NS equations were solved in the near-equilibrium regions while the rarefied flow regions were solved using the DSMC solver. For a single micronozzle flow case, the required computational time for our hybrid solver was about 68% of the individual DSMC simulator while the hybrid frame solution provided sufficient accuracies as much as the DSMC code accuracy. For the flow inside a micropropulsive system, we solved the channel and convergent section of the nozzle using the continuum solver and solved the divergent part of the nozzle and the buffer zone using the DSMC solver. The distinction between these two regions was provided using the local Knudsen number definition. We observed that there is a considerable static pressure reduction in the micropropulsion system if the splitter catalyst plates are inserted in the system. If the splitter plate's temperature is increased properly, the exit velocity and the specific impulse increase while the thrust force decreases. The velocity and temperature increase linearly as the flow passes over the high temperature splitter plates. Meanwhile, the Mach number gets the same value as that of using a low temperature splitter. Our investigation of nanopropulsion system showed that high viscous force effects do not permit the flow to reach the chocked state at the nozzle throat at nanoscales. In fact, the flow decelerates and heats before arriving the splitter plates. We concluded that the nano-scale propulsion systems are useful for lower propulsive force magnitude and can be recommended for use in orbital control purposes.

Acknowledgments

The authors would like to thank the financial support received from the Center for Research and Technology (Sharif University of Technology) and the Center for High-Technology Development (the Ministry of Industries and Business (Iran)) under contract no. 8795-S-006.

References

[1] G.A. Bird, Molecular Gas Dynamics and the Direct Simulation of Gas Flows, Clarendon Press, Oxford, 1994.
[2] R.L. Bayt, Analysis, fabrication and testing of a MEMS-based micropropulsion system, Ph.D. Dissertation, Massachusetts Institute of Technology, FDRLTR 99-1, 1999.
[3] I.D. Boyd, Y. Jafry, J. Van den Beukel, Investigation of nozzle and plume expansions of a small helium thruster, in: Proceedings of the 18th International Symposium on Rarefied Gas Dynamics, Washington, DC, 1994.
[4] Y. Jafry, J. Van den Beukel, Ultralow density plume measurements using a helium mass spectrometer, Journal of Vacuum Science and Technology 10 (4) (1992) 2642–2649.
[5] D. Zelesnik, M.M. Micci, L.N. Long, DSMC simulation of low Reynolds number nozzle flows, AIAA Paper 93-2490, in: 29th AIAA/SAE/ASME/ASEE Joint Propulsion Conference and Exhibit, Monterey, CA, 1999.
[6] M.S. Ivanov, G.N. Markelov, Numerical study of cold gas micronozzle flows, AIAA Paper 99-0166, in: 37th Aerospace Sciences Meeting & Exhibit, Reno, NV, 1999.
[7] D. Hitt, C.M. Zakrzwski, M.A. Thomas, MEMS-based satellite micropropulsion via catalyzed hydrogen peroxide decomposition, Smart Materials and Structures 10 (2001) 1163–1175.
[8] A.A. Alexeenko, D.A. Levin, S.F. Gimelshein, R.J. Collins, B.D. Reed, Numerical modeling of axisymmetric and three-dimensional flows in microelectromechanical systems nozzles, AIAA Journal 40 (5) (2002) 897–904.
[9] C. Xie, Characteristics of micronozzle gas flows, Physics of Fluids 19 (2007) 037102.
[10] E. Titov, A. Gallagher-Rogers, D. Levin, B. Reed, Examination of a collision-limiter direct simulation Monte Carlo method for micropropulsion applications, Journal of Propulsion and Power 24 (2) (2008) 311–321.
[11] F. La Torre, S. Kenjeres, C.R. Kleijn, P.A. Moerel, Effects of wavy surface roughness on the performance of micronozzles, Journal of Propulsion and Power 26 (4) (2010) 655–662.
[12] J.A. Moríñigo, J. Hermida-Quesada, Solid–gas surface effect on the performance of a MEMS-class nozzle for micropropulsion, Sensors and Actuators A: Physical 162 (1) (2010) 61–71.
[13] M. Darbandi, E. Roohi, Study of subsonic–supersonic gas flow through micro–nanoscale nozzles using unstructured DSMC solver, Microfluidics and Nanofluidics 10 (2) (2011) 321–335.
[14] M. Darbandi, G.E. Schneider, Momentum variable procedure for solving compressible and incompressible flows, AIAA Journal 35 (1997) 1801–1805.
[15] M. Darbandi, G.E. Schneider, Performance of an analogy-based all-speed procedure without any explicit damping, Computational Mechanics 26 (2000) 459–469.
[16] M. Darbandi, V. Mokarizadeh, A modified pressure-based algorithm to solve the flow fields with shock and expansion waves, Numerical Heat Transfer, Part B 46 (2004) 497–504.
[17] M. Darbandi, S. Vakilipour, Developing consistent inlet boundary conditions to study the entrance zone in microchannels, Journal of Thermophysics and Heat Transfer 21 (3) (2007) 596–607.
[18] M. Darbandi, E. Roohi, V. Mokarizadeh, Conceptual linearization of Euler governing equations to solve high speed compressible flow using a pressure-based method, Numerical Methods for Partial Differential Equations 24 (2) (2008) 583–604.
[19] S. Vakilipour, M. Darbandi, Advancement in numerical study of gas flow and heat transfer in microchannels, Journal of Thermophysics and Heat Transfer 23 (1) (2009) 205–208.
[20] M. Darbandi, S. Vakilipour, Solution of thermally developing zone in short micro/nano scale channels, Journal of Heat Transfer 131 (2009) 044501.
[21] E. Roohi, M. Darbandi, Extending the Navier–Stokes solutions to transition regime in two-dimensional micro-/nanochannel flows using information preservation scheme, Physics of Fluids 21 (2009) 082001.
[22] E. Roohi, M. Darbandi, V. Mirjalili, DSMC solution of subsonic flow through micro–nano scale channels, Journal of Heat Transfer 131 (9) (2009) 092402.
[23] E. Roohi, M. Darbandi, Recommendations on performance of parallel DSMC algorithm in solving subsonic nanoflows, Applied Mathematical Modeling 36 (5) (2012) 2314–2321.
[24] M. Darbandi, E. Roohi, DSMC simulation of subsonic flow through nanochannels and micro/nano steps, International Communication in Heat and Mass Transfer 38 (10) (2011) 1444–1449.
[25] T. Scanlon, E. Roohi, C. White, M. Darbandi, J. Reese, An open source, parallel DSMC code for rarefied gas flows in arbitrary geometries, Computers & Fluids 39 (2010) 2078–2089.
[26] OpenFOAM: The Open Source CFD Toolbox, User Guide, Version 2.01, OpenFOAM Foundation, 2011.
[27] I. Boyd, D.G. Chen, G.V. Candler, Predicting failure of the continuum fluid equations in transitional hypersonic flows, Physics of Fluids 7 (1995) 210–219.
[28] A.L. Garcia, J.B. Bell, W.Y. Crutchfield, B.J. Alder, Adaptive mesh and algorithm refinement using direct simulation Monte Carlo, Journal of Computational Physics 154 (1999) 134–139.

[29] T.E. Schwartzentruber, L.C. Scalabrin, I.D. Boyd, A modular particle–continuum numerical method for hypersonic non-equilibrium gas flows, Journal of Computational Physics 225 (2007) 1159–1174.
[30] M. Liu, X. Zhang, G. Zhang, Y. Chen, Study on micronozzle flow and propulsion performance using DSMC and continuum methods, Acta Mechanica Sinica 22 (2006) 409–416.
[31] F.J. Uribe, A.L. Garcia, Burnett description for plane Poiseuille flow, Physical Review E 60 (4) (1999) 4063–4078.

Biographies

Masoud Darbandi received his B.Sc. (heat and fluid) and M.Sc. (energy conversion) degrees from Sharif University of Technology (SUT), Tehran, Iran, in 1986 and 1989 respectively. He received his Ph.D. (computational fluid dynamics) from University of Waterloo (UW), Waterloo, Canada, in 1996. He was a post-doctoral research fellow in UW CFD group until 2000. In 1999, he joined the Aerospace Engineering Department of SUT as an assistant professor. He has been a full professor in SUT since 2007. His areas of interest include the CFD, the nanoscale, microscale, and continuous fluid flow and heat transfer simulations using the molecular, mesoscopic, and continuum- and semi-continuum-based methods. He has also been active in many industrial projects engaged with energy production, energy conversion, energy consumption, and their minimizations in different fluid flow and heat transfer applications.

Ehsan Roohi received his B.Sc. in aerospace engineering from Sharif University of Technology (SUT), Iran, in 2004, M.Sc. in mechanical engineering from Ferdowsi University of Mashhad (FUM), Iran, in 2006, and Ph.D. in aerospace engineering from SUT in 2010. This paper is a part of his Ph.D. research work titled as *Developing a Hybrid Molecular–Continuum Algorithm to Simulate Gas Flow in Micro–Nano Propulsion Systems*, which was supervised by Dr. Darbandi. He is currently an assistant professor in FUM. His area of interest is the low-speed and high-speed fluid flow simulations using CFD, DSMC, and Hybrid Methods.